Accepted Manuscript

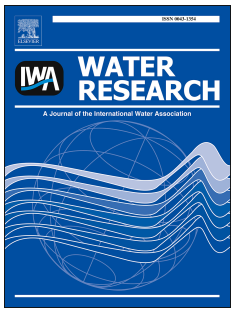

Highly efficient inactivation of bacteria found in drinking water using chitosan-bentonite composites: Modelling and breakthrough curve analysis

Sarah C. Motshekga, Suprakas Sinha Ray

PII: S0043-1354(17)30003-9

DOI: 10.1016/j.watres.2017.01.003

Reference: WR 12604

To appear in: *Water Research*

Received Date: 4 August 2016

Revised Date: 6 December 2016

Accepted Date: 2 January 2017

Please cite this article as: Motshekga, S.C., Ray, S.S., Highly efficient inactivation of bacteria found in drinking water using chitosan-bentonite composites: Modelling and breakthrough curve analysis, *Water Research* (2017), doi: 10.1016/j.watres.2017.01.003.

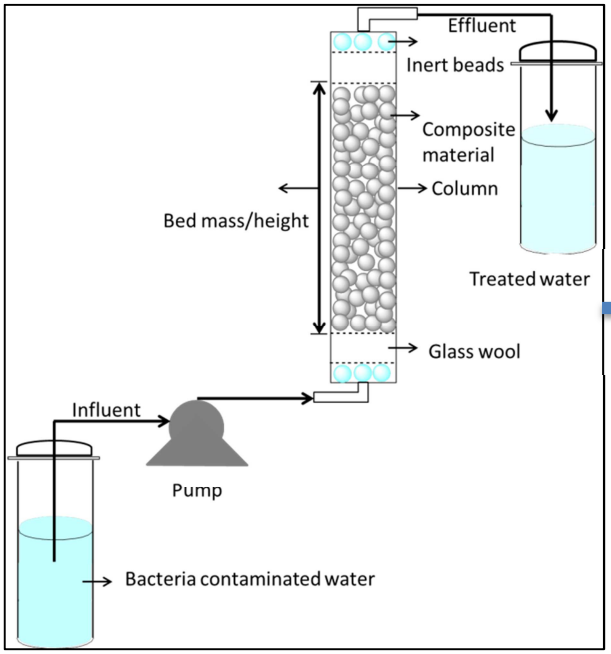

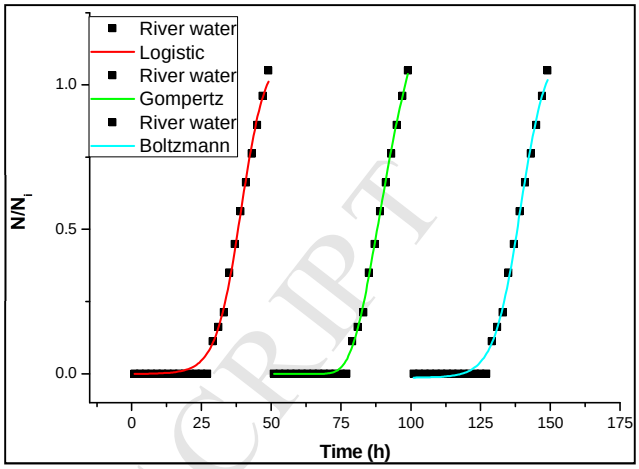

Highly efficient inactivation of bacteria found in drinking water using chitosan-bentonite composites: modelling and breakthrough curve analysis

Sarah C. Motshekga[a], *Suprakas Sinha Ray*[a,b*],

[a]DST-CSIR National Centre for Nanostructured Materials, Council for Scientific and Industrial Research, Pretoria 0001, South Africa

[b]Department of Applied Chemistry, University of Johannesburg, Doornfontein 2028, Johannesburg, South Africa

*****Corresponding author. E-mail: rsuprakas@csir.co.za; suprakas73@yahoo.com

Abstract

Disinfection of bacterially-contaminated drinking water requires a robust and effective technique and can be achieved by using an appropriate disinfectant material. The advanced use of nanomaterials is observed as an alternative and effective way for the disinfection process and water treatment as a whole. Hence, the inactivation of *Escherichia coli* (*E. coli*) using chitosan-Bentonite (Cts-Bent) composites was studied in a fixed bed column. Cts-Bent composites were synthesised using in situ cross-linking method using Bent-supported silver and zinc oxide nanoparticles. These composites were characterized by Fourier transform infrared spectroscopy, X-ray diffraction, scanning electron microscopy, and energy dispersive spectroscopy. The effect of the composite bed mass, initial concentration of bacteria, and flow rate on the bacterial inactivation was investigated. The characterization results revealed that the composites were successfully prepared and confirmed the presence of both silver and zinc oxide nanoparticles in the chitosan matrix. The growth curves of *E. coli* were expressed as breakthrough curves, based on the logistic, Gompertz, and Boltzmann models. The breakthrough time and processed volume of treated water at breakthrough were used as performance indicators, which revealed that the composites performed best at low bacterial concentration and flow rate and with substantial bed mass. The chitosan composites were found to be highly effective, which was demonstrated when no bacteria were observed in the effluent sample within the first 27 h of analysing river water. All

the models were suitable for adequately describing and reproducing the experimental data with a sigmoidal pattern. Therefore, the prepared composite is showing potential to work as a disinfectant and provide an alternative solution for water disinfection; hence this study should propel further research of the same or similar materials.

Keywords: chitosan-bentonite composites; fixed bed column; *Escherichia coli*; bacteria inactivation; disinfection models; breakthrough analysis

1. Introduction

Contamination of water sources by biological, chemical, and physical contaminants is a health threat to humans, living organisms, and the environment. Water quality continues to deteriorate; and as such, the problem needs to be addressed, as it constitutes a major public health issue. National and international guidelines for water quality have been implemented to meet the demand for safe drinking water. Due to the stringent water quality standards that have been adopted, cost effective and robust methods for water remediation are required. According to the World Health Organization (WHO), contaminated water leads to millions of deaths per year worldwide. In 2014, more than 840 000 adults and 360 000 children under the age of five died in developing countries, due to unsafe water supplies (WHO, 2014). Cholera outbreaks were reported in 2015, from parts of the African continent (Mozambique/Malawi, 2015; Wandiga, 2015). The WHO concluded that most of these diseases and deaths could have been prevented by increasing the availability of clean and safe water supplies.

Various chemical disinfection methods are available to control and improve the microbiological quality of drinking water, including chlorination, ozonation, chloramines, and ultraviolet radiation, as well as others (Richardson, 2003a, 2003b, 2004; Kraner et al., 2006; Li et al., 2008a). Whereas these methods are effective at inactivating bacterial contaminants to desired levels, some are often costly and time-consuming, produce harmful disinfection by-products (DBPs), or even require that a secondary disinfectant be used. Because of these concerns, more emphasis is being placed on

finding other alternative disinfectants that will require less processing time and not produce DBPs (Krasner et al., 2006), yet still meet the water quality requirements.

Advances in nanoscience and nanotechnology are promising in that most of the problems involving water quality issues could be solved using products based on them. Nanomaterials possess a broad range of enhanced physicochemical properties that make them attractive for use as reactive media for water treatment (Savage and Diallo, 2005; Warheit, 2008). These materials have large surface areas, small sizes, and increased reactivity that drastically enhance their usability for water treatment, which cannot be achieved by their bulky counterparts (Raghupathi et al., 2011). For instance, the antibacterial activity of metallic silver (Ag) has been known for centuries (Amato et al., 2011; Tartanson et al., 2014). This property originates from the silver ions that dissolve from the surface of the bulk Ag (Feng et al., 2000). Although silver ions are being used, bulk Ag is more advantageous, as the results are more stable and last longer. However, it is difficult to use bulk Ag in industrial or domestic applications because it is more expensive and has a low ion release rate (Feng et al., 2000).

Therefore, Ag nanoparticles (AgNPs), which have shown enhanced inactivation properties that bulk Ag cannot achieve, have been employed. The physicochemical properties of AgNPs are size-dependent, and AgNPs exhibit strong and enhanced antibacterial properties even when administered in small quantities (Warheit, 2008). In addition, nanomaterials can be functionalized with various chemical groups to improve their properties even further (Savage and Diallo, 2005). Under the nanotechnology umbrella, active research is being done to develop novel nanocomposites with increased selectivity towards different contaminants. Different nanocomposites are at various stages of research and development for the remediation of drinking water (Chong et al., 2011; Loo et al., 2013). These materials include antibacterial nanoparticles (Ag, zinc oxide (ZnO), copper oxide, magnesium oxide, etc.) (Ren et al., 2009; Rana and Kalaichelvan, 2011; Quang et al., 2013), magnetic nanoparticles (iron oxide) (Zhan et al., 2015), and carbonaceous materials (activated carbon, carbon nanotubes, graphene, etc.) (Li et al.; 2008b ;

Bao et al., 2011; Tuan et al., 2011; Sze and McKay, 2012), in addition to many others. At this stage, the key focus is on the preparation of composites containing nanoparticles and their antimicrobial properties. Although these composites are reported to be highly effective in the inactivation of various microorganisms, very few of these studies further continue to report on the use of the same composites for water disinfection (Amarjargal et al., 2013; Jin et al., 2013; Deng et al., 2014; Wehling et al., 2015; Deng et al., 2016; Pant et al., 2016; Saravanan et al., 2016; Xia et al., 2016; Zhang et al., 2016; Zhu et al., 2016). Some of these studies reported on the effectiveness of the composites to inactivate bacteria, either using the inhibition zone method or the batch method, which are the two preliminary methods, to test the antibacterial activities of the composites. The success of the inactivation results from these studies should propel and encourage further studies for water disinfection. For instance, Pant et al. (2016) prepared a multifunctional nanocomposite of silver-titanium nanoparticles supported on reduced graphene oxide for chemical and biological disinfection. In their study, the authors reported the nanocomposite to have been prepared by the simple and efficient method, which is economical and being non-toxic. The authors presented the nanocomposite to have superior antibacterial properties, and this was potential to be used in wastewater treatment. However, these studies were using both graphene/oxide and activated carbon as the supporting materials for the nanoparticles which are more expensive. Considering how difficult it may be to control the nanoparticle sizes and avoid agglomeration between the nanoparticles, this approach of supporting the nanoparticles on substrates is good as it allows a better dispersion of the nanoparticles and provides full usage of their properties. Introducing nanoparticles to these supports the result in composites of enhanced properties that can be used for various applications, therefore less expensive materials are needed. Clays and polymers make excellent supports for both metal and metal oxides nanoparticles. Environmental concerns and economic advantages are among the interests in clays, as they are abundantly accessible around the world. In this study, bentonite, clay from the smectite group was used to support the nanoparticles due to its high specific surface area, chemical stability and other

surface and structural properties (Juang et al., 2002). For these composites to effectively be applied in water disinfection, they were dispersed within a polymer matrix which helps in limiting the leaching rate of the nanoparticles into the water (Li et al., 2008). Polymers help in controlling the release rate of the nanoparticles from the matrix; hence a controlled amount is released. Chitosan, a biopolymer is the second most plentiful natural polymer that has been used in this study to effectively deliver the robust disinfection properties of the nanoparticle composites. Chitosan is less expensive, non-toxic and possesses inherent antimicrobial properties (Li et al., 2008; Raafat and Sahl, 2009; Kittinaovarat et al., 2010; Guibal et al., 2013).

Consequently, the objective of the current study was to evaluate the performance of chitosan composites in a continuous-flow fixed-bed column to inactivate bacteria. This is a continuation of our previous research study (Motshekga et al., 2015), which evaluated the performance of the composites using a batch mode method and provided fundamental information about the effectiveness of the composites based on the results. However, such data is not sufficient to be used for the design of water treatment systems where flow rate is an essential parameter for the water system. Hence, fixed bed column studies are essential because they are simple, produce good quality treated water, and provide additional information for the design of point-of-use water treatment systems. The continuous-flow fixed-bed process is also good for controlling and reducing the contaminant concentration in the effluent so it does not exceed the allowable limit. This can be achieved by varying the composite bed mass, initial bacterial concentration, and flow rate. To analyse the breakthrough curves (BTCs) of the experimental data, the logistic, Gompertz, and Boltzmann models were used to analyse the results. The correlation coefficient (R^2) predicted by the models was compared, to check which model best described the experimental data. The effectiveness of the composites was investigated using control water spiked with *Escherichia coli* (*E. coli*, ATCC 11775) and environmental water from the Apies River in South Africa.

2. Materials and methods

2.1. Materials

Pristine bentonite (Bent), which was used as a support for the Ag and ZnO nanoparticles, was obtained from Ecca Holdings (Pty) Ltd, South Africa. Chitosan (Cts) was purchased from Sigma Aldrich (South Africa) as a flake material. Glutaraldehyde (GLA, 50 wt% in H_2O); phosphate buffered saline (pH 7.4); sulphuric acid (98%); acetic acid (99%); sodium chloride; sodium hydroxide pellets (NaOH); silver nitrate (99.98%), which was used as the Ag precursor; and ZnO nanoparticles dispersed in ethanol were purchased from Sigma Aldrich, South Africa. All aqueous solutions were prepared using distilled water. Sodium thiosulfate and nutrient agar were purchased from Merck, South Africa. The bacterial strain used to provide the antibacterial activity was gram-negative *E. coli* (ATCC 11775) from the American Type Culture Collection, USA.

2.2. Synthesis of chitosan-bentonite (Cts-Bent) composite

The Cts-Bent composites were prepared as reported previously (Motshekga et al., 2015). Briefly, the Cts-Bent composites were obtained by mixing 1 g Bent-supported Ag and ZnO nanoparticles (Ag-ZnO/Bent) (Motshekga et al., 2013) into 250 ml of distilled water and stirring at 200 rpm for an hour at room temperature (25 ± 2 °C). Then, 250 ml of 1 wt% Cts solution was added to the Bent suspension and stirred at 500 rpm overnight. The mixture was then added to 1 M NaOH solution under gentle stirring and left overnight to neutralise the acid. The resulting Cts-Bent composites were rinsed extensively and filtered with distilled water to remove any residual NaOH. The wet Cts-Bent composites, now with irregular shape after filtering, were then dispersed in a 1% GLA solution and stirred overnight. The cross-linked Cts-Bent composites were washed extensively to remove any excess GLA solution. Finally, the composites were air dried at 30 °C for 4 h, followed by an increase in temperature to 70 °C at which they remained overnight. The Cts-Bent composites were crushed to a size of ≤ 1.7 mm.

2.3. Characterization of Cts-Bent composites

The surface morphology and dispersion of the Bent particles in the Cts matrix were explored using scanning electron microscopy (Zeiss Auriga SEM, Germany). The powdered samples were mounted on a copper stub using carbon tape and sputter coated with carbon to avoid charging.

Energy dispersive X-ray spectroscopy (EDS) analysis of the Cts-Bent composites was performed to obtain a qualitative determination of the elemental composition of the Ag and ZnO (as Zn) nanoparticles. For the crystalline phases, the samples were analysed with powdered X-ray diffraction (XRD, PANalytical X'PERT-PRO diffractometer, the Netherlands) measured using Ni-filtered CuKα radiation (λ = 1.5406 Å) and a variable slit at 35 kV and 50 mA. Fourier transform infrared (FTIR) spectra were recorded using a PerkinElmer Spectrum 100 (USA) spectrometer equipped with a germanium crystal. Leaching tests were performed to study the stability of the nanoparticles in the composites, which is of great importance, as this determines the suitability of the composites for water treatment. Into 20 mL of distilled water, 0.2 g of composite was added, and the mixture was shaken vigorously in a water-bath shaker (at 36 ± 1 °C, 200 rpm) for various lengths of time. After each shaking interval, a fraction of the water was withdrawn. The samples were analysed using inductively coupled plasma atomic emission spectroscopy (ICP-AES, PerkinElmer, USA) to determine the quantity of the nanoparticles that leached into the water.

2.4. Fixed-bed column experiment

Fixed-bed column experiments were performed in a small scale Plexiglas (acrylic) column with an internal diameter of 20 mm and length of 300 mm. The Cts-Bent composites were packed between glass wool and bracketed by inert glass beads at the upper and bottom ends of the column, which were closed using nylon caps. Prior to the column packing, the column tubes, column caps, and glass wool were sterilized using laminar flow under UV light, whereas the glass beads were sterilized using an autoclave. Control bacterial water with initial concentrations of 3×10^3, 5×10^3, and 1×10^4 cfu/mL was prepared and fed into the column at varying flow rates of 2, 5, and 10 mL/min. The control water was pumped continuously upwards into the column using a peristaltic pump. The effluent sample was then collected at hourly intervals in sterile, 2 mL Eppendorf tubes containing 15% sodium thiosulfate. After collection, petri dishes containing agar (plates) were inoculated with the samples. The plates were incubated at 37 °C for 24 h. The plates were prepared in triplicate and averages of such were reported. After incubation, the colonies that formed in each

plate were counted to express the bacterial concentrations as number of colony forming units per mL of sample (cfu/mL). The effects of bed mass, flow rate, and initial bacterial concentration were investigated.

2.5. Environmental water sampling and analysis

Environmental water samples were collected from the Apies River which is located in the Gauteng Province, South Africa. The Apies River flows through the city of Pretoria from the south northward until it meets with the Pienaars River. The water samples were collected aseptically using sterile bottles and transported on ice to the laboratory for physicochemical and microbiological analysis within 1–4 h of collection. The analyses were performed following the procedure recommended by the American Public Health Association (Standards Methods, 1998). The analyses of *E. coli*, *Salmonella* spp., and total and faecal coliforms were done following the procedure. To quantify the antibacterial efficiency of the Cts-Bent composites, column experiments were conducted as outlined in Section 2.4. Effluent samples were collected every hour, and the pour plate method was used to inoculate the samples into plates, which were then incubated at 37 °C for 24 h. The number of colonies in each plate was then counted to express the bacterial concentration in cfu/mL. Triplicate plates were prepared, and the averages of such were used. Final bacterial concentrations were calculated and expressed as cfu/mL, and the experimental data was expressed as N/N_i, with N being the concentration at time t and N_i, the initial bacterial concentration.

2.6. Modelling of breakthrough curves and data analysis

The performance of a fixed bed column is described through the concept of breakthrough curves. The breakthrough point is the time where bacteria are detected in the column effluent with a known concentration, whereas the breakthrough curve is the shape of the concentration-time profile (Ghasemi et al., 2011). The breakthrough point and curve are important characteristics for determining the process operation and response, because they affect the feasibility of the process design. In the present study, an attempt to evaluate the inactivation of bacteria through a fixed bed

column by mathematical models was performed based on the logistic, Gompertz, and Boltzmann models. Both the Gompertz and Boltzmann sigmoidal models are formulated from the logistic sigmoidal equation, which is an appropriate starting point for expressing phase transition phenomena. The proposed models can be used extensively to describe and understand the dynamics of fixed-bed growth curves for the inactivation of bacteria (Aksu et al., 2007; Ghasemi et al., 2011). The model effectiveness depends on the robustness of the inactivation process and the consumption of the disinfectant during the contact time (Gyürék and Finch, 1998). The amount of the effluent concentration and the growth curve were calculated by the logistic equation given as:

$$\frac{dN}{dt} = -Nk\left(1 - \frac{N}{N_i}\right) \qquad \text{(Eq. 1)}$$

where *k i*s the rate constant that describes the steepness of the slope and ≥ 0.

The equation becomes

$$\ln\left(\frac{N}{N_i - N}\right) = k(t - C) \text{ or } \ln\frac{N}{N_i} - \ln\left(1 - \frac{N}{N_i}\right) = kt + C \qquad \text{(Eq. 2)}$$

where N and N_i are the final and initial concentrations, respectively; t is time; and C is a constant equal to t_{50}, where t_{50} is the time required to reach the median concentration time.

For N number of colonies, the equation becomes:

$$N = \left(\frac{N_i}{1 + e^{k(t-C)}}\right). \qquad \text{(Eq. 3)}$$

Eq. 3 can be written as:

$$N = \left(\frac{N_i}{1 + e^{k(t-t_{50})}}\right) \qquad \text{(Eq. 4)}$$

The Gompertz equation can be expressed by the following equations:

$$\ln\ln\left(\frac{N}{N_i}\right) = -k(t - t_{50}) \qquad \text{(Eq. 5)}$$

$$N = N_i e^{-\exp(-k(t-t_{50}))} \quad \text{(Eq. 6)}$$

And the Boltzmann equation takes the form:

$$N = N_o + \frac{N_i - N_o}{1 + e^{\left(\frac{(t-t_{50})}{-k}\right)}} \quad \text{(Eq. 7)}$$

where N_o is the bottom concentration at time 0, which is commonly made a constant = 0.

Therefore, Eq. 7 reduces to:

$$N = \frac{N_i}{1 + e^{\left(\frac{(t-t_{50})}{-k}\right)}} \quad \text{(Eq. 8)}$$

3. Results and discussion

3.1. Morphology and formation of Cts-Bent composites

Fig. 1 presents the SEM micrographs of the Cts and Cts-Bent composites, showing the morphological differences between the two. **Fig. 1(a)** shows that Cts exhibited a smooth and uniform morphology, whereas the Cts-Bent composite (**Fig. 1(b)**) exhibited a rough morphology with numerous protruding bulk-like agglomerates, indicating the presence of Bent within the Cts matrix. The presence of Ag and ZnO nanoparticles was confirmed by EDS (**Fig. S1**, Supporting Information), because as expected, the EDS spectrum showed Ag and Zn peaks. Considerable Zn was recorded which approximated to 21 wt%, and, for Ag, a 1.7 wt% was recorded.

<**Fig. 1.** SEM micrographs of (a) chitosan and (b) Cts-Bent composites.>

The leaching results are presented in **Table 1**. The results revealed that both nanoparticles (Ag and ZnO) were released into the water, but were within the allowable limits recommended by the WHO. The acceptable concentrations for Ag and Zn in drinking water are set at 0.1 and 3−5 mg/L, respectively (WHO, 2011). Any water containing nanoparticles above these levels is neither suitable nor recommended for drinking. Therefore, with the acceptably small quantities that leached over a 12 h period, the composite could be suitable as an alternative disinfectant material, thus providing an affordable and environmentally friendly material for drinking water treatment.

<Table 1. Leaching results of Ag and ZnO (Zn) nanoparticles into the water (mg/L).>

XRD analyses were conducted to ascertain the formation of the Cts-Bent composites. **Fig. 2S** (Supporting Information) shows the presence of two broad peaks at 2θ = 6.94° and 20°, which indicate poor crystallinity of the chitosan. An XRD spectrum of chitosan is characterised by two sharp peaks at 2θ = 10° and 20°. Similar observations were reported in previous studies (Wang et al., 2005; Beppu et al., 2007; Li et al., 2013), in which the poor crystallinity of Cts was thought to have been caused by crosslinking with GLA. The peaks of Bent were observed at 2θ = 26° and 28°. Other peaks of Bent are usually observed at 2θ = 6°, 20°, and 35°, which overlapped with those of chitosan. All the peaks of Bent were corroborated in other published literature (Wang et al., 2005; Motshekga et al., 2013). Peaks confirming the presence of Ag were observed at 2θ = 35° and 62°, which are attributed to the crystallographic planes of the face-centred cubic silver crystals (Shameli et al., 2011; Quang and Chau, 2013). Other peaks observed at 2θ = 31.94°, 36.39°, 62.50°, and 68.60° were allocated to the wurtzite structure of hexagonal ZnO (Li et al., 2010; Raghupathi et al., 2011; Talebian et al., 2013). The observation of the peaks for Cts, Bent, and Ag and ZnO nanoparticles confirms the formation of the Cts-Bent composites.

Fig. 2 shows the FTIR spectra used to identify the functional groups present in the Cts-Bent composites. The strong broad band at 3338 cm^{-1}, which is evident in both the Cts and Cts-Bent composites, is assigned to the N-H stretching vibrations of $–NH_2$ groups. The band at 2885 cm^{-1} corresponds to the C-H stretching vibrations of $–CH_2$ groups, the bands at 1656 and 1559 cm^{-1} to N-H bending, the band at 1363 cm^{-1} to C-H bending, and the intense band at 1033 cm^{-1} is assigned to C-O stretching (Beppu et al., 2007; Li et al, 2013). The interlayered O-H group band at 3630 cm^{-1}, which originates from bentonite in the Cts-Bent composites, had a relatively low intensity. Other bands that correspond to Si-O-Si groups, which are characteristic of phyllosilicate minerals, were revealed at 1006 cm^{-1} and 796 cm^{-1}, in the absence of Cts (Motshekga et al., 2013). After the addition of Cts, the band at 1006 cm^{-1} shifted slightly to 1015 cm^{-1} and manifested as a very sharp band, whereas the band at 796 cm^{-1} remained the same. The bands for

278 $-NH_2$ groups appeared at 1656 and 1559 cm^{-1} for Cts. The band at 1656 cm^{-1} shifted to 1647 cm^{-1}
279 in the Cts-Bent composites, whereas the band at 1559 cm^{-1} remained in the same position but
280 exhibited reduced intensity (Shameli et al., 2010). Thus, the FTIR spectra reveal that all the
281 functional groups that could be expected from either Bent or Cts were observed. However, no
282 bands were observed for both Ag and ZnO nanoparticles in the Cts-Bent composite sample, as
283 indicated by the lack of difference between the Cts and Cts-Bent composite spectra. Bands of these
284 nanoparticles are said to be observed at the lower wavenumbers of the spectrum, but in this case,
285 their absence could be due to overlap with the bands of the Bent (Siqingaowa et al., 2006;
286 Chandrappa et al., 2010; Wankhede et al, 2013; Kutláková et al., 2015). Fig. 3S (Supporting
287 Information) shows the characteristic bands of the individual materials.

288 <**Fig. 2.** FTIR spectra of chitosan and chitosan-Bentonite composites.>

289 **3.2. Bacterial inactivation of control water and river water using Cts-Bent composites**

290 The inactivation efficiency of Cts-Bent composites was evaluated with control water and river
291 water through a fixed-bed column operation. Operational parameters, such as bed mass, flow rate,
292 and initial concentration of bacteria, were evaluated, as they are important for column design in
293 water treatment. The breakthrough results are discussed based on these parameters. The
294 mechanism in which the Cts-Bent composites exert their antibacterial activity is through Ag and
295 ZnO nanoparticles. The antibacterial property of Cts was not observed in this study because Cts is
296 reported to show its antibacterial activity at a lower pH (less than 6.0), where the positive amino
297 groups are charged (Li et al., 2008; Kong et al., 2010; Regiel et al., 2013). Although the
298 mechanism of both nanoparticles is still not well understood, it has been reported that the release
299 of the Ag^+ and Zn^{2+} by the active surfaces of Ag and ZnO nanoparticles, respectively, are the
300 biocidal agents which interact with the critical cell constituents causing disruption of the cell
301 contents, hence causing cell death. Additionally, the antibacterial activity not only relies on the
302 release of the nanoparticle ions, but also the high surface area to volume ratio in which the

nanoparticles bind on the surfaces of the bacteria and cause damage to the cell membrane (Li et al., 2008; Li et al., 2010; Xu et al., 2013; Biswas and Bandyopadhyaya, 2016; Haider et al., 2016)

3.2.1. Effect of bed mass on bacterial inactivation

Bed mass is an important parameter in evaluating the performance of bacterial inactivation particularly for a continuous system. The BTCs for the inactivation of *E. coli* by Cts-Bent composites with varying bed mass, fixed initial concentration of 5×10^3 cfu/mL, and flow rate of 5 mL/min are shown in **Fig. 3**, and the results are summarized in **Table 2**. As the bed mass increased, more active sites were available for contact with the water which resulted in higher inactivation efficiency of the bacteria. The results showed that the inactivation activity was highly dependent on the increase in bed mass, with the most inactivation occurring with the maximum of 15 g of the composite. The effect of mass was prominent, as the breakthrough and saturation times both increased, from 8 to 19 h and 46 to 51 h respectively, with increased bed mass. It is apparent that the bacterial inactivation increased rapidly with an increase in the amount of bed mass, due to an increase in the number of active sites and available surface area of the composite. The results also indicate that the volume of treated water at breakthrough varied with the bed mass. The breakthrough volume was 2.4, 3.6, and 5.7 L for bed mass loadings of 5, 10, and 15 g respectively. Furthermore, the bed mass became saturated more quickly with smaller mass loading, which corresponds to fewer active sites of the chitosan composite and smaller amounts of treated water. The R^2 values predicted by the three models were very high, which means the models fitted the experimental data very well (**Table 3**). The values increased with an increase in mass loading, showing that high mass loading was preferable to obtain good inactivation results. The Gompertz model was the best of the three models in reproducing the experimental data and gave decent goodness of fit (**Fig. 3**). Although the Boltzmann model was good in describing the experimental data, its goodness of fit at the initial phase (lag phase) was lacking, as demonstrated by an underestimation of the lag phase by immediately presenting an exponential phase, which

contrasted the experimental data. The logistic model also gave good results with high R^2 values and decent goodness of fit.

<**Fig. 3.** Breakthrough curves of *E. coli* inactivation using chitosan composites with varying bed masses of 5, 10, and 15 g and fixed initial bacterial concentration and flow rate of 5×10^3 cfu/mL and 5 mL/min respectively.>

<**Table 2.** Summary of breakthrough results for *E. coli* inactivation.>

<**Table 3.** Summary of parameters predicted from the logistic, Gompertz, and Boltzmann models for the inactivation of *E. coli*.>

3.2.2. Effect of flow rate on bacterial inactivation

To determine the effect of flow rate on bacterial inactivation, three flow rates of 2, 5, and 10 mL/min were used, with a fixed initial bacterial concentration of 5×10^3 cfu/mL and bed mass of 15 g. The BTCs are presented in **Fig. 4**, the results of which show that the use of high flow rates reduced the contact time between the composite and the water, thus allowing an earlier breakthrough time. This was observed as a reduced lag phase in the growth curves, where the phase was longer for the low flow rates and shorter with the high flow rate. With an increase in flow rate, the breakthrough time decreased from 9 to 4 h, whereas the saturation time decreased from 30 to 17 h. The volume of treated water as shown in **Table 2** increased with an increase in flow rate, and then decreased with a further increase in flow rate. This is because the breakthrough point was reached more quickly with a higher flow rate, because such a rate reduces the amount of treated water. The results show that a higher flow rate did not allow the column to perform well, as indicated by the low volume of processed water. The results also show that the medium flow rate of 5 mL/min is the optimum flow rate to use with the given parameters. In general, the volume of processed water at higher flow rates can be expected to be low, as high flow rates mean the contact time between the composite and the water is short, which leads to an early breakthrough. The BTCs show that the models fitted the experimental data well (**Table 3**), as the growth curves were closer to the experimental ones from the lag phases to the stationary phases. With a higher flow

rate, the models failed to describe the experimental data fully. The best goodness of fit for the models was observed with the lowest flow rate of 2 mL/min, and as the flow rate increased, the models failed to reproduce the experimental data. Although there was a lack of decent goodness of fit in reproducing the experimental data with precision, the R^2 values were high for all the models. Furthermore, the R^2 values decreased with an increase in flow rate for all the models.

<**Fig. 4.** Breakthrough curves of *E. coli* inactivation using chitosan composites with varying flow rates of 2, 5, and 10 mL/min and fixed initial bacterial concentration and bed mass of 5×10^3 cfu/mL and 15 g respectively.>

3.2.3. Effect of initial bacterial concentration on bacterial inactivation

The effect of initial bacterial concentration was studied using a fixed bed mass of 15 g and flow rate of 5 mL/min by varying the bacterial concentrations to 3×10^3, 5×10^3, and 1×10^4 cfu/mL. The BTCs are presented in **Fig. 5**. As the bacterial concentration increased, the breakthrough time decreased from 15 to 5 h. This is because, as the bacterial concentration increases, the availability of active sites are reduced as more composite is needed, which leads to the breakthrough and saturation times being reached more quickly. In addition, the volume of treated water at breakthrough was reduced considerably as the initial bacterial concentration increased. As expected, the low bacterial concentration had a later breakthrough time, and the volume of treated water was greater, when compared to the high bacterial concentration. The predicted model parameters are presented in **Table 3**. The BTCs of the models showed that the best goodness of fit occurred with the lowest bacterial concentration of 3×10^3 cfu/mL, and it started to decrease with the highest concentration of 1×10^4 cfu/mL. The goodness of fit by the Boltzmann model failed dismally to reproduce the lag phase of the experimental data at the higher concentrations. The model produced a straight line at the highest bacterial concentration of 1×10^4 cfu/mL and an R^2 value of 0.9971. This observation of a straight line was observed for all three models at this concentration. This means that the experimental growth curves were not adequately reproduced by the models, especially for the lag phase. However, the R^2 values were very high which indicates

that despite not giving decent goodness of fit for the lag phase, the models were still accurate in describing the experimental data.

<**Fig. 5.** Breakthrough curves of *E. coli* inactivation using Cts-Bent composites with varying initial bacterial concentrations of 3×10^3, 5×10^3, and 1×10^4 cfu/mL and fixed bed mass and flow rate of 15 g and 5 mL/min respectively.>

3.3. Inactivation model comparison

The reliability and accuracy of the selected models were assessed by the R^2 values and the goodness of fit of the experimental data. The goodness of fit of the growth curves to the experimental data showed the accuracy of the models to sufficiently predict the bacterial responses, whereas the high R^2 values indicated that all the models predicted and reproduced the experimental data very well. The models were very competitive, with all $R^2 \geq 0.9715$. The slight differences in model fitting confirmed the variations in the model equations or were the result of model overfitting. Fakruddin *et al*. (2011) reported in their study that models usually predict faster growth rates than what is observed, which makes them respond in a fail-safe manner. Therefore, the models often tend to overestimate the experimental data. From the BTCs predicted by the models in this study, the stationary phases were merely observed, whereas the lag phases, in most instances, were underestimated. Therefore, the findings of the present study corroborate what Fakruddin *et al.* (2011) reported. Both the logistic and Gompertz models described the experimental data very well, whereas the Boltzmann model underestimated the lag phase. The stationary phase results may be due to the experiments being stopped immediately after the bed mass reached its saturation point, resulting in a short duration of this phase. For all the other phases, the models reproduced the experimental data with accuracy. Another considerable aspect in modelling is that, although the BTCs predicted by the models might deviate from the experimental data, it does not mean the model is defective. Rather, it implies that more knowledge is needed because other factors or parameters used in the model development are affecting the growth curve behaviour (Fakruddin *et al*., 2011).

3.4. River water analysis and bacterial inactivation

The physicochemical properties of the sampled river water are summarized in **Table 4**. The analyses show that the river water was within the recommended physical and chemical limits for drinking water (SANS 241:1 (2011); WHO (2011)). The temperature and pH ranges of 22.3 ± 0.56 °C and 7.6 ± 0.82, respectively, and the turbidity of 0.25 NTU were nonthreatening. The chloride, sulphate, and fluoride concentrations of 31, 36, and < 0.2 mg/L, respectively, were also found to be within acceptable limits. These analysed physicochemical properties suggested that the water did not pose a threat to the health of the consumers, as stipulated by the SANS 241:1 (2011) and WHO (2011).

<**Table 4.** Analysis of physicochemical and microbiological water quality of the Apies River.>

However, the water showed poor microbiological quality, as shown by the viable counts of *E. coli* and faecal and total coliforms (**Table 4**). These counts exceeded the maximum recommended limit for no risk, which raises concern about how vulnerable the consumers of this water source are because of the poor microbiological quality of the water. The water was also tested for *Salmonella* and 0 viable counts per 100 mL of sample were found. Whereas indicator organisms may not necessarily be pathogenic, their presence increases the risk of having pathogenic bacteria. Observations of high levels of indicator organisms indicate the potential presence of pathogenic bacteria that are frequently known to cause waterborne diseases such as outbreaks of diarrhoea. But in this study, for instance, the pathogenic *Salmonella* was not observed even though high counts of *E. coli* and faecal and total coliforms were observed.

Because of the high counts of the indicator organisms after repeated isolations, the river water was analysed with the composites to investigate the capability of the composites to inactivate the bacteria in the river water through a continuous-flow fixed-bed column. The results showed that the composites were highly effective, with no viable counts of any bacteria detected in the effluent sample. In fact, no bacteria were detected in the effluent sample in the first 27 h of running the column at 5 mL/min with 15 g of bed mass. Viable counts were observed after more water passed

through the composites (after 27 h) and increased as the bed mass became saturated. These results show that the Cts-Bent composite inactivated the bacteria in both the control water and the river water. It should be noted that the initial bacterial concentrations of the control water were very high when compared to what would normally be found in river water. This was done purposely to test the efficiency of the composites in inactivating bacteria at higher concentrations. Therefore, the results suggest that the composites are suitable enough to use for bacterial inactivation, and that the high inactivation efficiency should be expected with bacterial concentrations as high as $1x10^4$ cfu/mL.

The breakthrough time and volume of processed water at breakthrough were used to evaluate the inactivation performance of the composites. The breakthrough time was reached after 27 h with a breakthrough volume of 8.1 L, and saturation time was reached after 47 h. The logistic, Gompertz, and Boltzmann models were used to predict the performance of the composites (**Fig. 6**). All the models described the experimental data perfectly well with high R^2 values of 0.9945, 0.9979, and 0.9950 for the logistic, Gompertz, and Boltzmann models, respectively. The goodness of fit was also very good for all the models, as corroborated by the high R^2 values. The models described the experimental data with great precision, as shown by the accuracy of the experimental growth curves and reproducing of the data from the lag phase to the stationary phase. All the disinfection profile curves (lag phase, exponential phase, and stationary phase) were well described by the models, as shown by their sigmoidal patterns.

<Fig. 6. Breakthrough curves of bacterial inactivation using Cts-Bent composites with river water, at a fixed mass load and flow rate of 15 g and 5 mL/min respectively.>

4. Conclusions

- The Cts-Bent composites were successfully synthesized by the in situ cross-linking method to effectively inactivate bacteria in controlled water and river water.

- The chitosan ensured that the nanoparticles were anchored around/within the polymer matrix which administers a controlled release of the nanoparticles to inactivate bacteria either by contact or release of the nanoparticle ions.
- The inactivation of bacteria using both controlled water and river water was evident, as was determined by the lack of viable counts in the effluent sample after 27 h of continuous column operation with river water. Compared with other disinfectants, the cost implication of the materials allows for a large-scale production of the composites that can be used in rural communities especially where they rely on river water for their daily needs. These results imply that the composites are promising to work as a disinfectant and could be used for water treatment systems.
- Furthermore, the concentration of the control water employed in the study was typically higher from what would normally be found from the environmental water; hence the composites would be expected to perform excellently in a water treatment system using environmental water.

Acknowledgements

The authors wish to thank the Department of Science and Technology and the Council for Scientific and Industrial Research, South Africa, for their financial support.

REFERENCES

Aksu, Z., Cagatay, S.S., Gonen, F., 2007. Continuous fixed bed biosorption of reactive dyes by dried Rhizopus arrhizus: Determination of column capacity. Journal of Hazardous Materials 143, 362–371.

Amato, E., Diaz-Fernandez, Y.A., Taglietti, A., Pallavicini, P., Pasotti, L., Cucca, L., Milanese, C., Grisoli, P., Cesare, D., 2011. Synthesis, characterization and antibacterial activity against Gram positive and Gram negative bacteria of biomimetically coated silver nanoparticles. Langmuir 27, 9165–9173.

Amarjargal, A., Tijing L.D., Im, I.T., Kim, C.S., 2013. Simultaneous preparation of Ag/Fe_3O_4 core–shell nanocomposites with enhanced magnetic moment and strong antibacterial and catalytic properties. Chemical Engineering Journal 226 (2013), 243–254.

Bao, Q., Zhang, D., Qi, P., 2011. Synthesis and characterization of silver nanoparticle and graphene oxide nanosheet composites as a bactericidal agent for water disinfection. Journal of Colloid and Interface Science 360 (2), 463–470.

Beppu, M.M., Vieira, R.S., Aimoli, C.G., Santana, C.C., 2007. Crosslinking of chitosan membranes using glutaraldehyde: Effect on ion permeability and water absorption. Journal of Membrane Science 301, 126–130.

Biswas, P., Bandyopadhyaya, R., 2016. Water disinfection using silver nanoparticle impregnated activated carbon: *Escherichia coli* cell-killing in batch and continuous packed column operation over a long duration. Water Research 100, 105–115.

Chandrappa, K.G., Venkatesha, T.P., Vathsala, K., Shivakumara, C., 2010. A hybrid electrochemical–thermal method for the preparation of large ZnO nanoparticles. Journal of Nanoparticle Research 12, 2667–2678.

Chong, M.N., Jin, B., Saint, C.P., 2011. Bacterial inactivation kinetics of a photo-disinfection system using novel titania-impregnated kaolinite photocatalyst. Chemical Engineering Journal 171, 16–23

Deng, C.H., Gong, J.L., Zeng, G.M., Niu, C.G., Niu, Q.Y., Zhang, W., Liu, H.Y., 2014. Inactivation performance and mechanism of *Escherichia coli* inaqueous system exposed to iron oxide loaded graphene nanocomposites. Journal of Hazardous Materials 276, 66–76.

Deng, C.H., Gong, J.L., Zeng, G.M., Jiang, Y., Zhang, C., Liu, H.Y., Huan, S.Y., 2016. Graphene–CdS nanocomposite inactivation performance toward *Escherichia coli* in the presence of humic acid under visible light irradiation. Chemical Engineering Journal 284, 41–53.

Fakruddin, M., Mazumder, R.M., Mannan, K.S.B., 2011. Predictive microbiology: Modeling microbial responses in food. Ceylon Journal of Science (Biological Science) 40, 121−131.

Feng, Q.L., Wu, J., Chen, G.Q., Cui, F.Z., Kim, T.N., Kim J.O., 2000. A mechanistic study of the antibacterial effect of silver ions on *Escherichia coli* and *Staphylococcus aureus*. Journal of Biomedical Materials Research 52, 662−668.

Ghasemi, M., Keshtkar, A.L., Dabbagh, R., Safdari, S.J., (2011). Biosorption of uranium (VI) from aqueous solutions by Ca-pretreated Cystoseira indica alga: Breakthrough curves studies and modelling. Journal of Hazardous Materials 189, 141–149.

Guibal, E., Cambe, S., Bayle, S., Taulemesse, J.M., Vincent, T. (2013). Silver/chitosan/cellulose fibers foam composites: From synthesis to antibacterial properties. Journal of Colloid and Interface Science 393, 411–420.

Gyürék, L.L., Finch, G.R., (1998). Modeling water treatment chemical disinfection kinetics. Journal of Environmental Engineering 124, 783−793.

Haider, M.S., Shao, G.N., Imran, S.M., Park, S.S., Abbas, N., Tahir, M.S., Hussain, M., Bae, W., Kim, H.T., 2016. Aminated polyethersulfone-silver nanoparticles (AgNPs-APES) composite membranes with controlled silver ion release for antibacterial and water treatment applications. Materials Science and Engineering C 62, 732–745.

Jin, Y., Dai, Z., Liu, F., Kim, H., Tong, M., Hou, Y., 2013. Bactericidal mechanisms of Ag_2O/TNBs under both dark and light conditions. Water Research 47, 1837–1847.

Juang, R.S.; Lin, S.H.; Tsao, K.H., (2002). Mechanism of the sorption of phenols from aqueous solutions onto surfactant-modified montmorillonite. Journal of Colloid Interface Science 254, 234–241.

Kong, M., Chen, X.G., Xing, K., Park, H.J., 2010. Antimicrobial properties of chitosan and mode of action: a state of the art review. International Journal of Food Microbiology 144, 51–63.

Kittinaovarat, S., Kansomwan, P., Jiratumnukul, N., 2010. Chitosan/modified montmorillonite beads and adsorption Reactive Red 120. Applied Clay Science 48, 87–91.

Krasner, S.W., Weinberg, H.S., Richardson ,S.D., Pastor, S.J., Chinn, R.; Sclimenti, M.J., Onstad, G.D., Thruston Jr., A.D., (2006). Occurrence of a new generation of disinfection by-products. Environmental Science and Technology 40, 7175–7185.

Kutláková, K.M., Tokarský, J., Peikertová, P., (2015). Functional and eco-friendly nanocomposite kaolinite/ZnO with high photocatalytic activity. Applied Catalysis B: Environmental 162, 392–400.

Li, Q., Mahendra, S., Lyon, D.Y., Brunet, L.Y., Liga, M.V., Li, D., Alvarez, P.J.J., (2008). Antimicrobial nanomaterials for water disinfection and microbial control: Potential applications and implications. Water research 42, 4591– 4602.

Li, L.H., Deng, J.C., Deng, H.R., Liu, Z.L., Li, X.L., (2010). Preparation, characterization and antimicrobial activities of chitosan/Ag/ZnO blend films. Chemical Engineering Journal 160, 378–382.

Li, B., Shan, C.L., Zhou, Q., Fang. Y., Wang, Y.L., Xu. F., Han L.R., Ibrahim, M., Guo, L.B., Xie, G.L., Sun, G.C., 2013. Synthesis, characterization, and antibacterial activity of cross-linked chitosan-glutaraldehyde. Marine Drugs 11, 1534–1552.

Loo, S.-L., Fane, A. G., Lim, T.-T., Krantz, W. B., Liang, Y.-N., Liu, X., Hu, X., 2013. Superabsorbent cryogels decorated with silver nanoparticles as a novel water technology for point-of-use disinfection. Environmental Science & Technology 47, 9363–9371.

Motshekga, S.C., Ray, S.S., Onyango, M.S., Momba, M.N.B., 2013. Microwave-assisted synthesis, characterization and antibacterial activity of Ag/ZnO nanoparticles supported bentonite clay. Journal of Hazardous Materials 262, 439–446.

Motshekga, S.C, Ray, S.S., Onyango, M.S., Momba, M.N.B., 2015. Preparation and antibacterial activity of chitosan-based nanocomposites containing bentonite supported silver and zinc oxide nanoparticles for water disinfection. Applied Clay Science 114, 330–339.

Mozambique/Malawi: Cholera Outbreak - Feb 2015. http://reliefweb.int/disaster/ep-2015-000015-moz. Accessed March 2016.

Pant, B., Saud, P.S., Park, M., Park, S.J., Kim, H.Y., 2016. General one-pot strategy to prepare Ag-TiO_2 decorated reduced graphene oxide nanocomposites for chemical and biological disinfectant. Journal of Alloys and Compounds 671, 51–59.

Quang, D.V., Sarawade, P.B., Jeon, S.J., Kim, S.H., Kim, J-K., Chai Y.G., Kim, H.T., 2013a. Effective water disinfection using silver nanoparticle containing silica beads. Applied Surface Science 266, 280–287.

Quang, D.V., Chau, N.H., 2013b. The Effect of hydrothermal treatment on silver nanoparticles stabilized by chitosan and its possible application to produce mesoporous silver powder. Journal of Powder Technology 2013, 1−6.

Raafat, D., Sahl, H.G., (2009). Chitosan and its antimicrobial potential – a critical literature survey. Microbial Biotechnology 2, 186–201.

Raghupathi, K.R., Koodali, R.T., Manna, A.C., 2011. Size-dependent bacterial growth inhibition and mechanism of antibacterial activity of zinc oxide nanoparticles. Langmuir 27, 4020–4028.

Rana, S., Kalaichelvan, P.T. 2011. Antibacterial Activities of Metal Nanoparticles. Advanced Biotechlogy 11, 21−23.

Regiel, A., Irusta, S., Kyzioł, A., Arruebo, M., Santamaria, J., 2013. Preparation and characterization of chitosan–silver nanocomposite films and their antibacterial activity against Staphylococcus aureus. Nanotechnology 24, 1–13.

Ren, G., Hu, D., Cheng, E.W.C., Vargas-Reus, M.A., Reip, P., Allaker, R.P, 2009. Characterisation of copper oxide nanoparticles for antimicrobial applications. International Journal of Antimicrobial Agents 33, 587−590.

Richardson, S.D., 2003a. Disinfection by-products and other emerging contaminants in drinking water. Trends in Analytical Chemistry 22, 666−684.

584 Richardson, S.D., 2003b. Water analysis: Emerging contaminants and current Issues. Analytical
585 Chemistry 75, 2831−2857.
586 Richardson S.D., 2004. Environmental mass spectrometry: Emerging contaminants and current
587 issues. Analytical Chemistry 76, 3337−3364.
588 Saravanan, A., Kumar, P.S., Devi, G.K., Arumugam, T., 2016. Synthesis and characterization of
589 metallic nanoparticles impregnated onto activated carbon using leaf extract of Mukia
590 maderasapatna: Evaluation of antimicrobial activities. Microbial Pathogenesis 97, 198–203.
591 Savage, N., Diallo, M.S., 2005. Nanomaterials and water purification: Opportunities and
592 challenges. Journal of Nanoparticle Research **7**, 331−342.
593 SANS 241-1:2011 Edition 1. Drinking Water. Part 1: Microbiological, physical, aesthetic and
594 chemical determinants. South African National Standards. Published by SABS Division, South
595 Africa 1−24.
596 Shameli, K., Ahmad, M.B., Zin, W.M., Yunus, W., Rustaiyan, A., Ibrahim, N.A, Zargar, M.,
597 Abdollahi, Y., 2010. Green synthesis of silver/montmorillonite/chitosan bionanocomposites using
598 the UV irradiation method and evaluation of antibacterial activity. International Journal of
599 Nanomedicine 5, 875–887.
600 Shameli, K., Ahmad, M.B., Zargar, M., Yunus, W.M.Z.W., Ibrahim, N.A., Shabanzadeh, P.,
601 Moghaddam, M.G., 2011. Synthesis and characterization of silver/montmorillonite/chitosan
602 bionanocomposites by chemical reduction method and their antibacterial activity. International
603 Journal of Nanomedicine 2011, 271–284.
604 Siqingaowa, Z., Yao, H., Garidi. 2006. Preparation and characterization of nanocrystalline ZnO by
605 direct precipitation method. Frontiers of Chemistry in China 1, 277−280.
606 Standard Methods for Examination of Water and Wastewater. (1998). 20th Ed., AWWA, Water
607 Environment Federation, APHA, Washington, DC, USA.
608 Sze, M.F.F., Mckay, G., 2012. Enhanced mitigation of para-chlorophenol using stratified activated
609 carbon adsorption columns. Water Research 46, 700–710.

Talebian, N., Amininezhad, S.M., Doudi, M., 2013. Controllable synthesis of ZnO nanoparticles and their morphology-dependent antibacterial and optical properties. Journal of Photochemistry and Photobiology B: Biology 120, 66–73.

Tartanson, M. A., Soussan, L., Rivallin, M., Chis, C., Penaranda, D., Lapergue, R., Calmels, P., Faur, C., 2014. A new silver based composite material for SPA water disinfection. Water Research 63, 135–146.

Tuan, T.Q., Son, N.V., Dung, H.T.K., Luong, N.H., Thuy, B.T., Anh, N.T.V., Hoa, N.D., Hai, N.H., 2011. Preparation and properties of silver nanoparticles loaded in activated carbon for biological and environmental applications. Journal of Hazardous Materials 192, 1321–1329.

Wandiga, S.O., 2015. Critical Water Issues in Africa. Book Chapter. Chapter 6. Water Challenges and Solutions on a Global Scale. ACS Publications, 95−113.

Wang, S.F., Shen, L., Tong, Y.J., Chen, L., Phang, I.Y., Lim, P.Q., Liu, T.X., 2005. Biopolymer chitosan/montmorillonite nanocomposites: Preparation and characterization. Polymer Degradation and Stability 90, 123−131.

Wankhede, Y.B, Kondawar, S.B., Thakare, S.R., More, P.S., 2013. Synthesis and characterization of silver nanoparticles embedded in polyaniline nanocomposite. Advanced Materials Letters 4, 89−93.

Warheit, D.B., 2008. Toxicological high light how meaningful are the results of nanotoxicity studies in the absence of adequate material characterization? Toxicological Sciences 101, 183–185.

Wehling, J., Köser, J., Lindner, P., Lüder, C., Beutel, S., Kroll, S., Rezwan, K., 2015. Silver nanoparticle-doped zirconia capillaries for enhanced bacterial filtration. Materials Science and Engineering C 48, 179–187.

WHO, 2011. Guidelines for drinking-water Quality, 4th Ed. vol. 1. World Health Organization, Geneva, Switzerland.

635 WHO, 2014. Preventing diarrhoea through better water, sanitation and hygiene: exposures and
636 impacts in low- and middle-income countries. World Health Organization, Geneva, Switzerland.
637 Xia, D., An, T., Li, G., Wang, W., Zhao, H., Wong, P.K., 2016. Synergistic photocatalytic
638 inactivation mechanisms of bacteria by graphene sheets grafted plasmonic Ag–AgX (X = Cl, Br, I)
639 composite photocatalyst under visible light irradiation. Water Research 99, 149–161.
640 Zhan, S., Zhu, D., Ma, S., Yu, W., Jia, Y., Li, Y., Yu, H., Shen, Z., 2015. Highly efficient removal
641 of pathogenic bacteria with magnetic graphene composite. ACS Applied Materials & Interfaces 7,
642 4290–4298.
643 Zhang, H.Z., Zhang, C., Zeng, G.M., Gong, J.L., Ou, X.M., Huan, S.Y., 2016. Easily separated
644 silver nanoparticle-decorated magnetic graphene oxide: Synthesis and high antibacterial activity.
645 Journal of Colloid and Interface Science 471, 94–102.
646 Zhu, X., Wu, D., Wang, W., Tan, F., Wong, P.K., Wang, X., Qiu, X., Qiao, X., 2016. Highly
647 effective antibacterial activity and synergistic effect of Ag-MgO nanocomposite against
648 *Escherichia coli*. Journal of Alloys and Compounds 684, 282–290.

Table 1. Leaching results of Ag and ZnO (Zn) nanoparticles into the water (mg/L)

Sample	NPs	0 min	0.5 h	1 h	4 h	12 h
Ag-Cts-Bent	Ag	<0.005	0.010	0.023	0.050	0.069
ZnO-Cts-Bent	Zn	<0.020	0.270	0.160	0.180	0.220
Ag/ZnO-Cts-Bent	Ag	<0.005	0.008	0.011	0.023	0.022
	Zn	<0.020	<0.02	0.047	0.440	0.460

Table 2. Summary of breakthrough results for *E. coli* inactivation

	Quantity	Breakthrough time (h)	Saturation time (h)	Time required to reach median concentration (t_{50}) (h)	Volume at breakthrough (L)	Volume at saturation (L)
Mass effect	5 g	8	46	27	2.4	13.8
	10 g	12	48	37	3.6	14.4
	15 g	19	51	41	5.7	15.3
Flow rate effect	2 mL/min	9	43	30	1.08	5.16
	5 mL/min	9	34	22	2.7	10.2
	10 mL/min	4	30	17	2.4	18
Initial bacterial concentration	3×10^3 cfu/mL	15	41	31	4.5	12.3
	5×10^3 cfu/mL	10	46	33	3	13.8
	1×10^4 cfu/mL	5	54	30	1.5	16.2

Table 3. Summary of parameters predicted from the logistic, Gompertz, and Boltzmann models for the inactivation of *E. coli*.

	Quantity	Logistic model		Gompertz model		Boltzmann model	
		K (h^{-1})	R^2	K (h^{-1})	R^2	K (h^{-1})	R^2
Mass effect	5 g	0.1308	0.9715	0.0699	0.9831	17.5689	0.9849
	10 g	0.1039	0.9795	0.0392	0.9861	19.7518	0.9881
	15 g	0.1429	0.9954	0.0484	0.9972	7.8931	0.9964
Flow rate effect	2 mL/min	0.1611	0.9948	0.0692	0.9972	7.2586	0.9962
	5 mL/min	0.2227	0.9931	0.1104	0.9977	5.4117	0.9958
	10 mL/min	0.2190	0.9872	0.1094	0.9944	7.5301	0.9944
Initial bacterial concentration	3×10^3 cfu/mL	0.1941	0.9952	0.0780	0.9970	5.6237	0.9959
	5×10^3 cfu/mL	0.1115	0.9847	0.0429	0.9901	17.8530	0.9926
	1×10^4 cfu/mL	0.1087	0.9919	0.0561	0.9965	14.2411	0.9977

Table 4. Analysis of physicochemical and microbiological water quality of the Apies River

	Units	**Sampled water value**	**Guideline value**
Escherichia coli	cfu/mL	12	Not detected
Faecal coliforms	cfu/mL	55	Not detected
Total coliforms	cfu/mL	80	≤ 10
Salmonella spp.	cfu/mL	Absent/100 mL	Not detected
Temperature	°C	22.8 ± 0.56	≤ 15
pH value	pH units	7.6 ± 0.36	≥ 5 to ≤ 9.7
Turbidity	NTU	0.25	≤ 1
Calcium	mg/L Ca	31	< 150
Chloride	mg/L Cl	31	≤ 300
Fluoride	mg/L F	< 0.2	≤ 1.5
Magnesium	mg/L Mg	18	< 70
Nitrates	mg/L N	2.7	≤ 11
Sulphates	mg/L SO_4	36	≤ 500

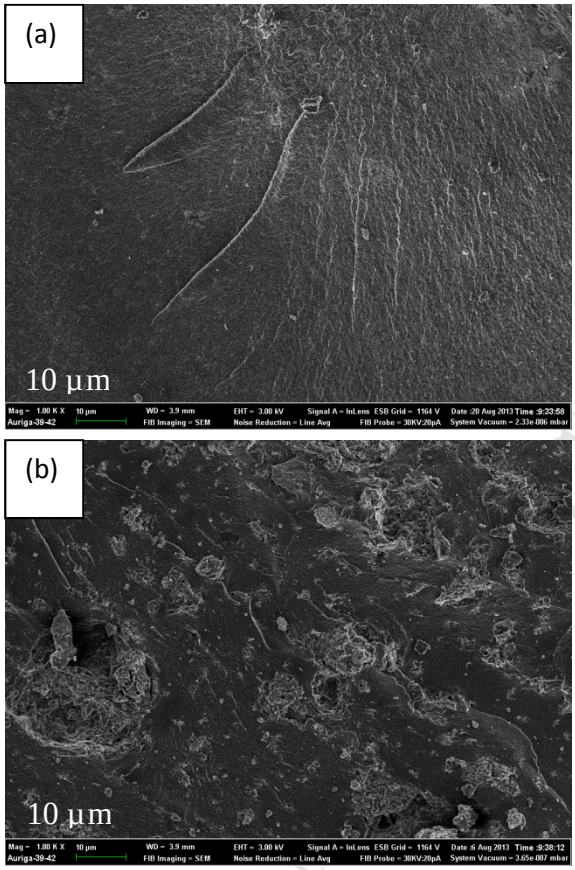

Fig. 1. SEM micrographs of (a) chitosan and (b) Cts-Bent composites.

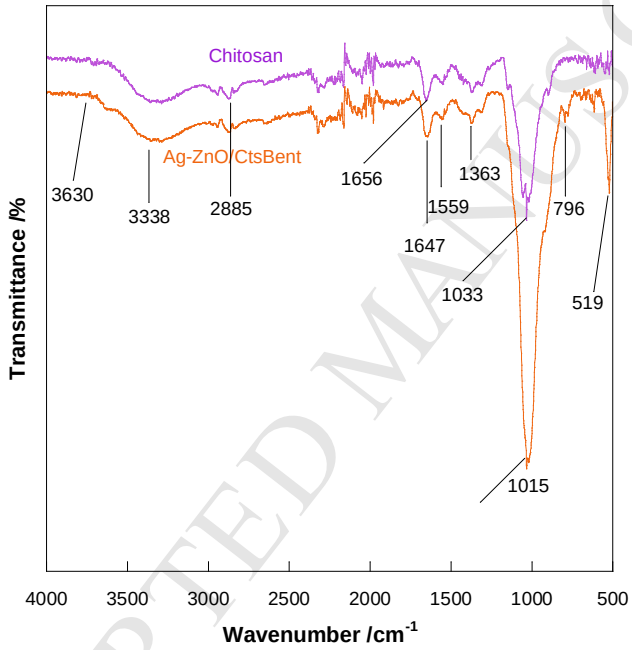

Fig. 2. FTIR spectra of chitosan and chitosan-Bentonite composites.

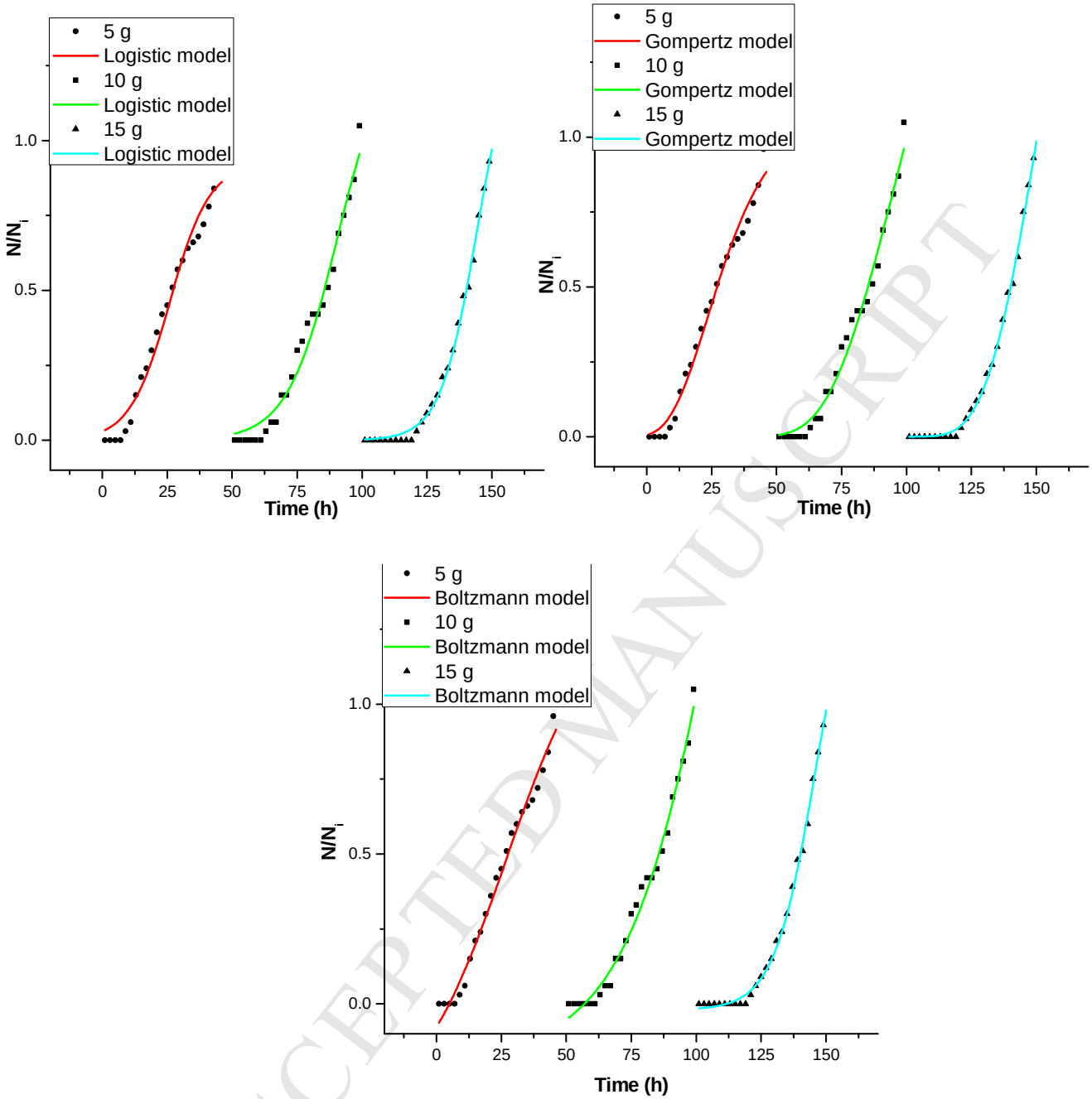

Fig. 3. Breakthrough curves of *E. coli* inactivation using chitosan composites with varying bed masses of 5, 10, and 15 g and fixed initial bacterial concentration and flow rate of 5×10^3 cfu/mL and 5 mL/min respectively.

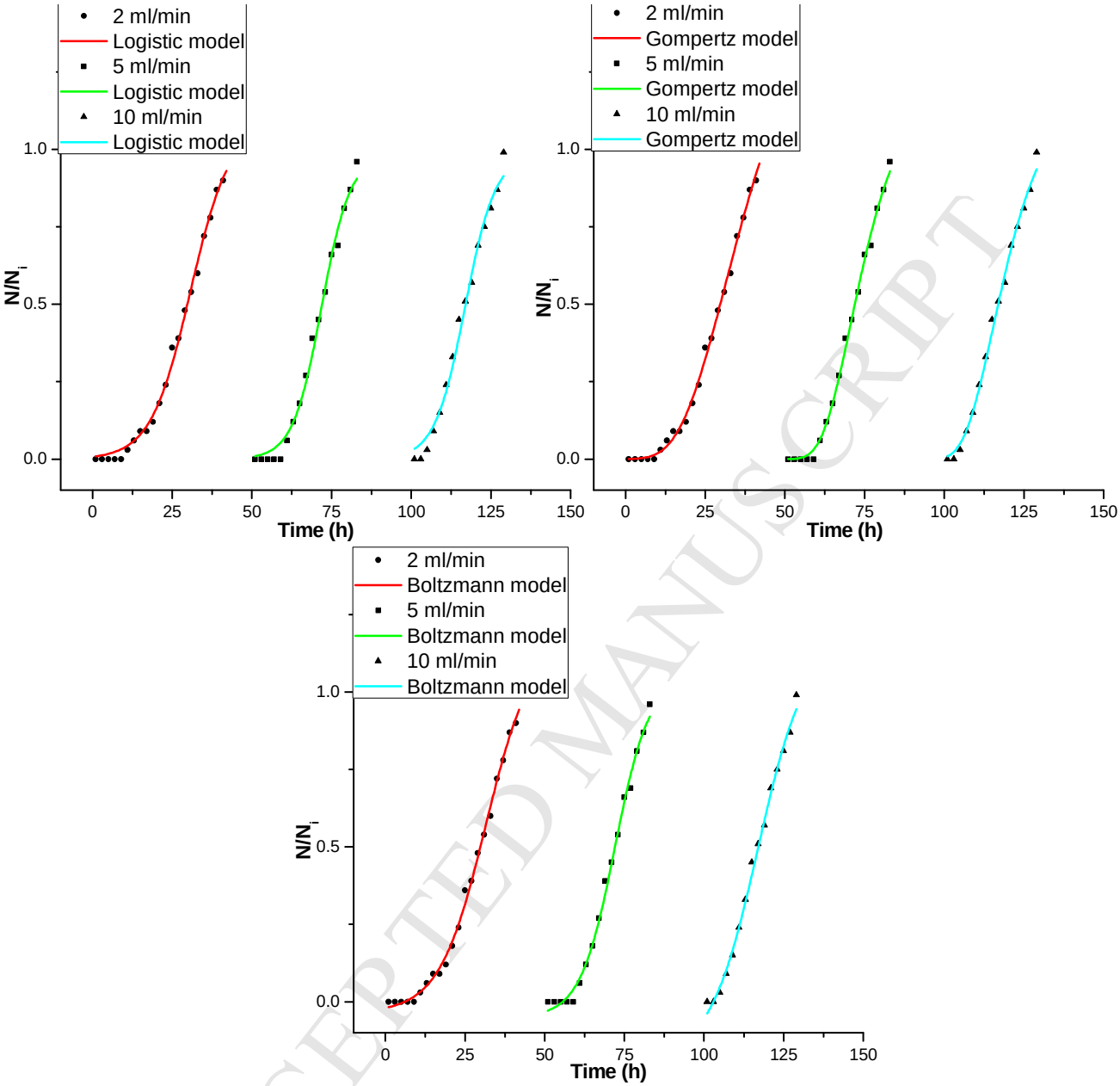

Fig. 4. Breakthrough curves of *E. coli* inactivation using chitosan composites with varying flow rates of 2, 5, and 10 mL/min and fixed initial bacterial concentration and bed mass of 5 × 10^3 cfu/mL and 15 g respectively.

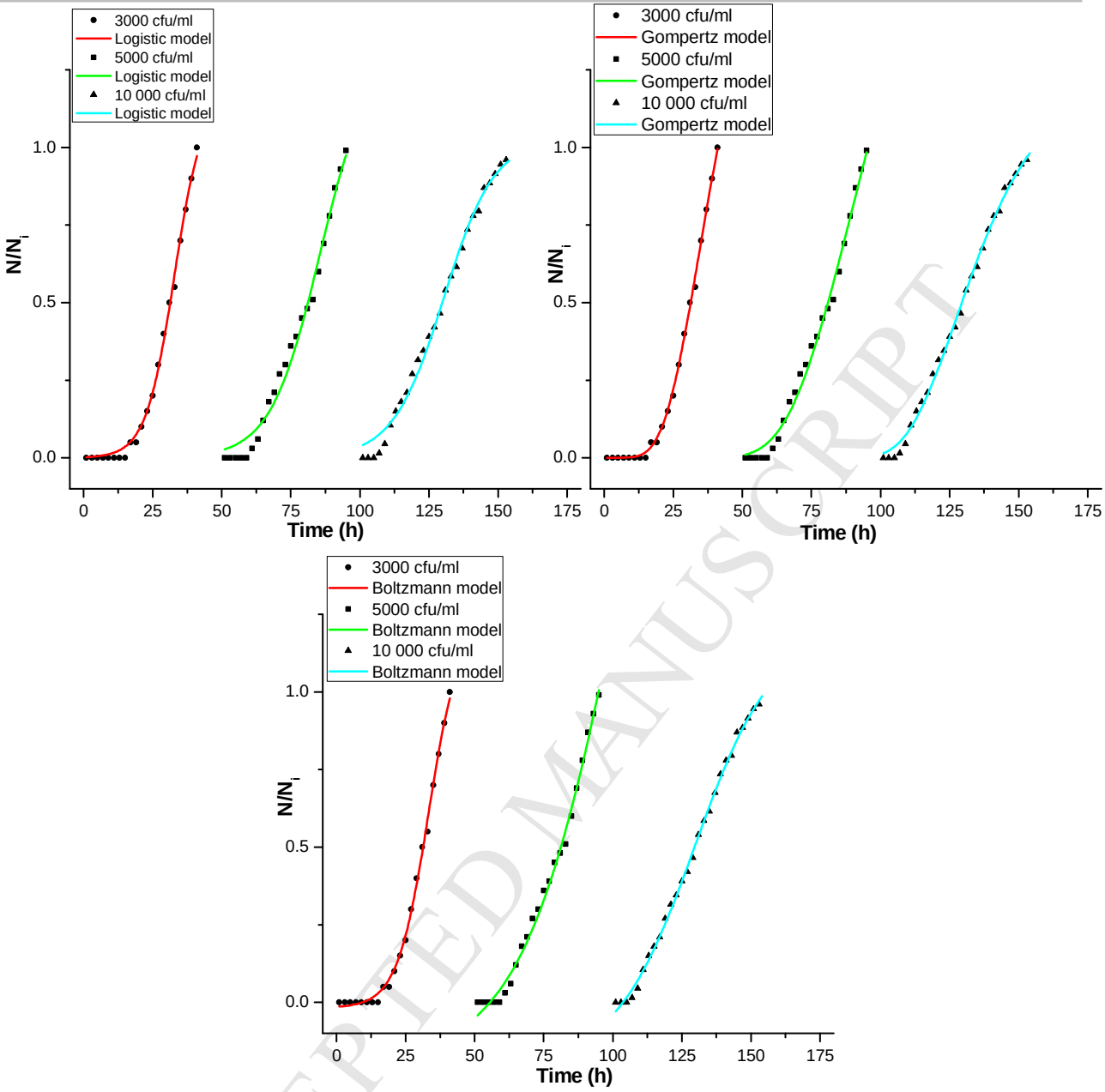

Fig. 5. Breakthrough curves of *E. coli* inactivation using Cts-Bent composites with varying initial bacterial concentrations of 3×10^3, 5×10^3, and 1×10^4 cfu/mL and fixed bed mass and flow rate of 15 g and 5 mL/min respectively.

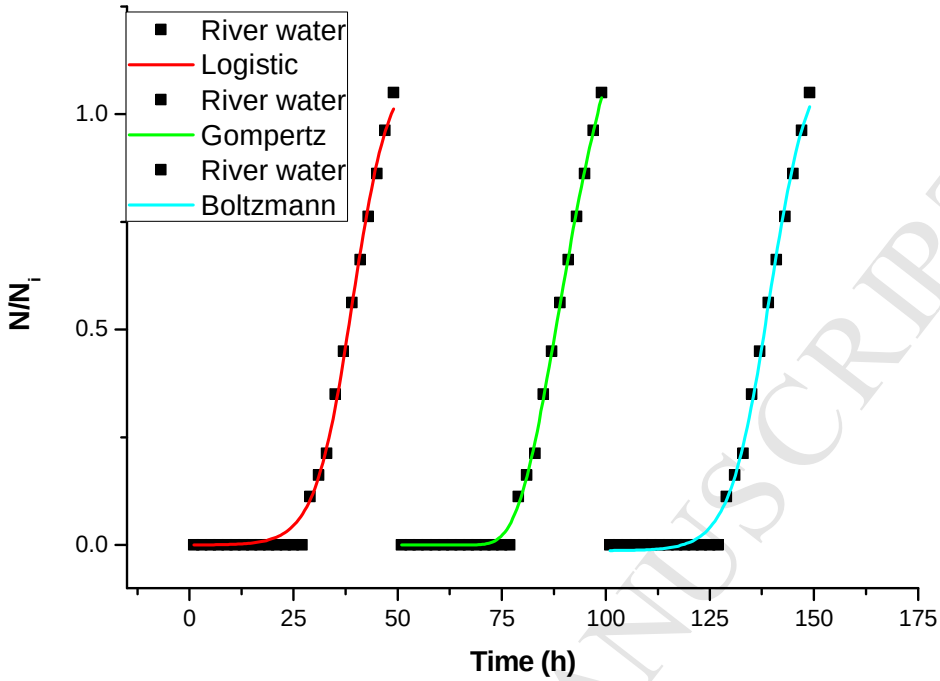

Fig. 6. Breakthrough curves of bacterial inactivation using Cts-Bent composites with river water, at a fixed mass load and flow rate of 15 g and 5 mL/min respectively.

Manuscript Highlights

- Chitosan composites provide an alternative solution for water disinfection
- Performance of chitosan composites through fixed bed column was investigated
- High efficient bacterial inactivation by chitosan composites
- Disinfection models describe experimental data adequately
- No bacteria was observed in the effluent sample within the first 27 hours